

# The Influence of Temperature on Ozone Production under varying NO<sub>x</sub> Conditions – a modelling study

J. Coates<sup>1</sup>, K. Mar<sup>1</sup> and T. Butler<sup>1</sup>

<sup>1</sup>Institute for Advanced Sustainability Studies, Potsdam, Germany

February 10, 2016

## Abstract

Ground-level ozone is a secondary air pollutant produced during the degradation of emitted volatile organic compounds (VOCs) and nitrogen oxides (NO<sub>x</sub>) in the presence of sunlight. As ozone production is dependent on photochemical processes, meteorological factors such as temperature influence ozone production. Temperature directly influences ozone production through speeding up the rates of the chemical processes producing ozone and increasing the emissions of VOCs, such as isoprene, from vegetation. In this study, we used a box model to reproduce the non-linear relationship of ozone on NO<sub>x</sub> and temperature from previous observational studies. Faster chemistry was responsible for an increase in ozone of up to 20 ppbv while increased isoprene emissions added a further 11 ppbv of ozone under high-NO<sub>x</sub> conditions. The shorter lifetime of peroxy nitrates with increased temperature was the main contributor to the increased production of ozone with temperature. At 40 °C, the thermal decomposition of peroxy nitrates was responsible for up to 45 % of the normalised O<sub>x</sub> production. The rate of increase in ozone with temperature from our box model simulations was about half rate of the increase in ozone with temperature over central Europe compared to both observed and WRF-Chem simulations. The missing sensitivity in our simulations compared to observations and 3D model output is related to the indirect influence of temperature on ozone production not included in our experiment.

## 1 Introduction

Surface-level ozone (O<sub>3</sub>) is a secondary air pollutant formed during the photochemical degradation of volatile organic compounds (VOCs) in the presence of nitrogen oxides (NO<sub>x</sub>  $\equiv$  NO + NO<sub>2</sub>). Due

to the photochemical nature of ozone production, meteorological variables such as temperature strongly influence ozone production (Jacob and Winner, 2009). Otero et al. (2016) showed that temperature was a major meteorological driver for summertime ozone in many areas of central Europe.

Temperature primarily influences ozone production in two ways: speeding up the reaction rates of many chemical reactions leading to ozone production and increasing emissions of VOCs from biogenic sources (BVOCs). In general, emissions of anthropogenic VOCs (AVOCs) are not typically dependent on temperature, however evaporative emissions of AVOCs increase with temperature (Rubin et al., 2006). The review of Pusede et al. (2015) provides further details of the temperature-dependent processes impacting ozone production.

Studies over the US (Sillman and Samson, 1995; Dawson et al., 2007; Pusede et al., 2014) noted that increased temperatures tend to lead to higher ozone levels, often exceeding local air quality guidelines. Some studies (Sillman and Samson, 1995; Dawson et al., 2007) included regional modelling to simulate the observed increases in ozone with temperature. In these studies, the increase of ozone with temperature was attributed to the shorter lifetime of PAN (peroxy acetyl nitrate) at higher temperatures and increased emissions of BVOCs, in particular isoprene, from vegetation.

Pusede et al. (2014) used an analytical model constrained by observations over San Joaquin Valley, California to infer a non-linear relationship of ozone production with temperature and  $\text{NO}_x$ , similar to the well-known non-linear relationship of ozone production on  $\text{NO}_x$  and VOC levels (Sillman, 1999). Moreover, Pusede et al. (2014) showed that temperature can be used as a surrogate for VOC levels when considering the relationship of ozone across  $\text{NO}_x$  gradients.

Environmental chamber studies have also been used to analyse the relationship of ozone with temperature. The chamber experiments of Carter et al. (1979) and Hatakeyama et al. (1991) showed increases in ozone from a VOC mix with temperature linked to increased PAN decomposition at temperatures greater than 303 K.

Despite many studies considering the effects of temperature on ozone production from an observational and chamber study perspective, there are no modelling studies (to our knowledge) focusing on the detailed chemical processes of the influence of temperature on ozone production across  $\text{NO}_x$  gradients. Regional modelling studies have concentrated on reproducing ozone levels over regions with known meteorology and  $\text{NO}_x$  conditions then only varying the temperature. These modelling studies did not consider the relationship of ozone with  $\text{NO}_x$  with temperature.

The review of Pusede et al. (2015) also highlights a lack of modelling studies looking at the non-linear relationship of ozone on temperature across  $\text{NO}_x$  gradients.

In this study, we use an idealised box model to determine how ozone levels vary with temperature across  $\text{NO}_x$  gradients. We determine whether faster chemistry or increased BVOC emissions have a greater influence on instantaneous ozone production with higher temperature at different  $\text{NO}_x$  conditions. Rasmussen et al. (2013) indicated that changing the chemical mechanism used by a model may also change the simulated ozone-temperature relationship to investigate this, we repeated all simulations using various chemical mechanisms.

## 2 Methodology

### 2.1 Model Setup

We used the MECCA box model to determine the important gas-phase chemical processes for ozone production under different temperatures and  $\text{NO}_x$  conditions. The MECCA box model was set up as described in Coates and Butler (2015) and updated to include vertical mixing with the free troposphere using a diurnal cycle for the PBL height. The supplementary material includes further details of these updates.

Simulations were performed to broadly simulate urban conditions of central Europe with equinoctical conditions. The simulations started at 06:00 with a total run time of two days. Methane was fixed at 1.7 ppmv throughout the model run, carbon monoxide (CO) and ozone were initialised at 200 ppbv and 40 ppbv and then allowed to evolve freely throughout the simulation. All VOC emissions were held constant until noon of first day simulating a plume of freshly-emitted VOC.

Separate box model simulations were performed by systematically varying the temperature between 288 and 313 K (15 – 40 °C). The only source of  $\text{NO}_x$  emissions in the box model was a constant source of NO emissions. Box model runs were performed with the NO emissions systematically varied between  $5.0 \times 10^9$  and  $1.5 \times 10^{12}$  molecules (NO)  $\text{cm}^{-2} \text{ s}^{-1}$  at each temperature used in this study. At 20 °C, these NO emissions corresponded to peak  $\text{NO}_x$  mixing ratios of 0.02 ppbv and 10 ppbv respectively, this range of  $\text{NO}_x$  mixing ratios covers the  $\text{NO}_x$  conditions in pristine and urban conditions (von Schneidemesser et al., 2015b).

Model runs were repeated using a temperature-dependent and temperature-independent source of BVOC emissions to determine whether increased emissions of BVOC or faster chemistry

Table 1: Total AVOC emissions in 2011 in tonnes from each SNAP category assigned from TNO-MACC\_III emission inventory and temperature-independent BVOC emissions in tonnes from Benelux region assigned from EMEP. The allocation of these emissions to MCMv3.2, CRIv2, CB05, MOZART-4 and RADM2 species are found in the supplementary material.

	<b>SNAP1</b>	<b>SNAP2</b>	<b>SNAP34</b>	<b>SNAP5</b>	<b>SNAP6</b>	<b>SNAP71</b>
Belgium	4494	9034	22152	5448	42809	6592
Netherlands	9140	12173	29177	8723	53535	16589
Luxembourg	121	44	208	1371	4482	1740
Total	13755	21251	62648	15542	100826	24921
	<b>SNAP72</b>	<b>SNAP73</b>	<b>SNAP74</b>	<b>SNAP8</b>	<b>SNAP9</b>	<b>BVOC</b>
Belgium	2446	144	210	6448	821	7042
Netherlands	3230	1283	1793	10067	521	1462
Luxembourg	1051	6	324	643	0	2198
Total	6727	1433	2327	17158	1342	10702

is more important for the increase of ozone with temperature. MEGAN2.1 (Guenther et al., 2012) specified the temperature-dependent BVOC emissions of isoprene, Sect. 2.3 provides further details. As isoprene emissions are the most important on the global scale, we considered only isoprene emissions from vegetation (Guenther et al., 2006). Only isoprene emissions were dependent on temperature, all other emissions were constant in all simulations. In reality, many other BVOC are emitted from varying vegetation types (Guenther et al., 2006) and increased temperature can also increase AVOC emissions through increased evaporation (Rubin et al., 2006).

All simulations were repeated using different chemical mechanisms to investigate whether the relationship of ozone with temperature across  $\text{NO}_x$  gradients changes using different representations of ozone production chemistry. The reference chemical mechanism was the near-explicit Master Chemical Mechanism, MCMv3.2, (Jenkin et al., 1997, 2003; Saunders et al., 2003; Rickard et al., 2015). The reduced chemical mechanisms in our study were Common Representative Intermediates, CRIv2 (Jenkin et al., 2008), Model for ozone and related chemical tracers, MOZART-4 (Emmons et al., 2010), Regional Acid Deposition Model, RADM2 (Stockwell et al., 1990) and the Carbon Bond Mechanism, CB05 (Yarwood et al., 2005). Coates and Butler (2015) described these chemical mechanisms and the implementation of these chemical mechanisms in MECCA. These reduced chemical mechanisms were chosen as they are commonly used by modelling groups in 3D regional and global models (Baklanov et al., 2014).

## 2.2 VOC Emissions

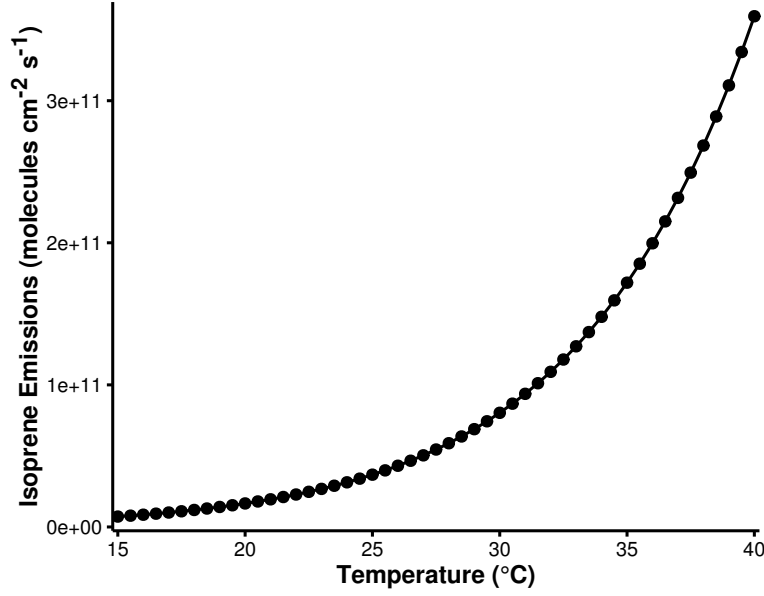
Emissions of urban AVOC over central Europe were taken from TNO-MACC\_III emission inventory for the Benelux (Belgium, Netherlands and Luxembourg) region for the year 2011. TNO-MACC\_III is the updated TNO-MACC\_II emission inventory created using the same methodology as Kuenen et al. (2014) and based upon improvements to the existing emission inventory during AQMEII-2 (Pouliot et al., 2015).

Temperature-independent emissions of isoprene and monoterpenes from biogenic sources were calculated as a fraction of the total AVOC emissions from each country in the Benelux region. This data was obtained from the supplementary data available from the EMEP (European Monitoring and Evaluation Programme) model (Simpson et al., 2012). Temperature-dependent emissions of isoprene are detailed in Sect. 2.3.

AVOC emissions were allocated to SNAP (Selected Nomenclature for Air Pollution) source categories. Table 1 shows the quantity of VOC emissions from each SNAP category and the temperature-independent BVOC emissions. These categorised AVOC emissions were assigned to chemical species and groups based on the country specific profiles for Belgium, the Netherlands and Luxembourg provided by TNO. Most individual chemical species are represented by the MCMv3.2, otherwise the individual contributions of a group of VOC were further split into individual components using the detailed speciation of Passant (2002). For example, ‘xylenes’ are one of the component chemical groups in many SNAP categories but the MCMv3.2 treats xylenes as the individual isomers (m-, o-, p-xylene) and the contributions of the individual isomers to a SNAP category was provided by Passant (2002). This approach was also used in von Schneidemesser et al. (2015a) to allocate AVOC emissions from different solvent sector speciations to MCMv3.2 species.

The VOC emissions represented by the MCMv3.2 were mapped to the mechanism species representing VOC emissions in each reduced chemical mechanism based on the recommendations of the source literature and Carter (2015). The VOC emissions in the reduced chemical mechanisms were weighted by the carbon numbers of the MCMv3.2 species and the emitted mechanism species, thus keeping the amount of emitted carbon constant between simulations. The supplementary data outlines the primary VOC and calculated emissions with each chemical mechanism.

Figure 1: The estimated isoprene emissions (molecules isoprene  $\text{cm}^{-2} \text{s}^{-1}$ ) using MEGAN2.1 at each temperature used in the study.



## 2.3 Temperature Dependent Isoprene Emissions

Temperature-dependent emissions of isoprene were estimated using the MEGAN2.1 algorithm for calculating the emissions of VOC from vegetation (Guenther et al., 2012). Emissions from nature are dependent on variables including temperature, radiation and age but for the purpose of our study all variables except temperature were held constant.

The MEGAN2.1 parameters were chosen to give similar isoprene mixing ratios at 20 °C to the temperature-independent emissions of isoprene in order to compare the effects of increased isoprene emissions with temperature. The estimated emissions of isoprene with MEGAN2.1 using these assumptions are illustrated in Fig. 1 and show the expected exponential increase in isoprene emissions with temperature (Guenther et al., 2006).

The estimated emissions of isoprene at 20 °C lead to 0.07 ppbv of isoprene in our simulations while at 30 °C, the increased emissions of isoprene using MEGAN2.1 estimations lead to 0.35 ppbv of isoprene in the model. A measurement campaign over Essen, Germany (Wagner and Kuttler, 2014) measured 0.1 ppbv of isoprene at temperature 20 °C and 0.3 ppbv of isoprene were measured at 30 °C. The similarity of the simulated and observed isoprene mixing ratios indicates that the MEGAN2.1 variables chosen for calculating the temperature-dependent emissions of isoprene were suitable for simulating urban conditions over central Europe.

Table 2: Increase in ozone mixing ratio (ppbv) due to chemistry and emissions at 40 °C from reference temperature (20 °C) in the NO<sub>x</sub>-regimes of Fig. 3.

Chemical Mechanism	Source of Difference	Increase in Ozone at 40 °C from 20 °C (ppbv)		
		Low-NO <sub>x</sub>	Maximal-O <sub>3</sub>	High-NO <sub>x</sub>
MCMv3.2	Chemistry	6.8	12.5	15.2
	Emissions	4.6	7.7	10.6
CRIV2	Chemistry	6.0	11.1	13.7
	Emissions	4.8	7.9	10.8
MOZART-4	Chemistry	6.0	10.2	12.3
	Emissions	4.1	6.7	10.0
CB05	Chemistry	9.3	16.0	19.9
	Emissions	4.6	7.4	9.8
RADM2	Chemistry	8.6	14.1	17.3
	Emissions	3.8	5.7	7.8

### 3 Results and Discussion

#### 3.1 Ozone as a Function of NO<sub>x</sub> and Temperature

Figure 2 depicts the maximum mixing ratio of ozone as a function of the total NO<sub>x</sub> emissions on the first day of simulations and temperature when using a temperature-independent and temperature-dependent source of isoprene emissions for each chemical mechanism. A non-linear relationship of ozone mixing ratios with NO<sub>x</sub> and temperature is reproduced by each chemical mechanism. This non-linear relationship is similar to that determined by Pusede et al. (2014) using an analytical model constrained to observational measurements over the San Joaquin Valley in California.

Higher ozone mixing ratios are produced when using a temperature-dependent source of isoprene emissions (Fig. 2). The highest mixing ratios of ozone are produced at high temperatures and high emissions of NO<sub>x</sub> regardless of the source of isoprene emissions. Conversely, the least amount of ozone is produced with low emissions of NO<sub>x</sub> over the whole temperature range (15 – 40 °C) when using both a temperature-independent and temperature-dependent source of isoprene emissions.

The contours of ozone mixing ratios as a function of NO<sub>x</sub> and temperature can be split into three NO<sub>x</sub> regimes (Low-NO<sub>x</sub>, Maximal-O<sub>3</sub> and High-NO<sub>x</sub>), similar to the NO<sub>x</sub> regimes defined for the non-linear relationship of ozone with VOC and NO<sub>x</sub>. The Low-NO<sub>x</sub> regime corresponds to regions with little increase in ozone with temperature, also called the NO<sub>x</sub>-sensitive regime. The High-NO<sub>x</sub> (or NO<sub>x</sub>-saturated) regime is when ozone levels increase rapidly with temperature and the contour ridges correspond to regions of maximal ozone production and we call this the

Figure 2: Contours of maximum ozone mixing ratios (ppbv) as a function of the total  $\text{NO}_x$  emissions on the first day and temperature for each chemical mechanism using a temperature-dependent and temperature-independent source of isoprene emissions.

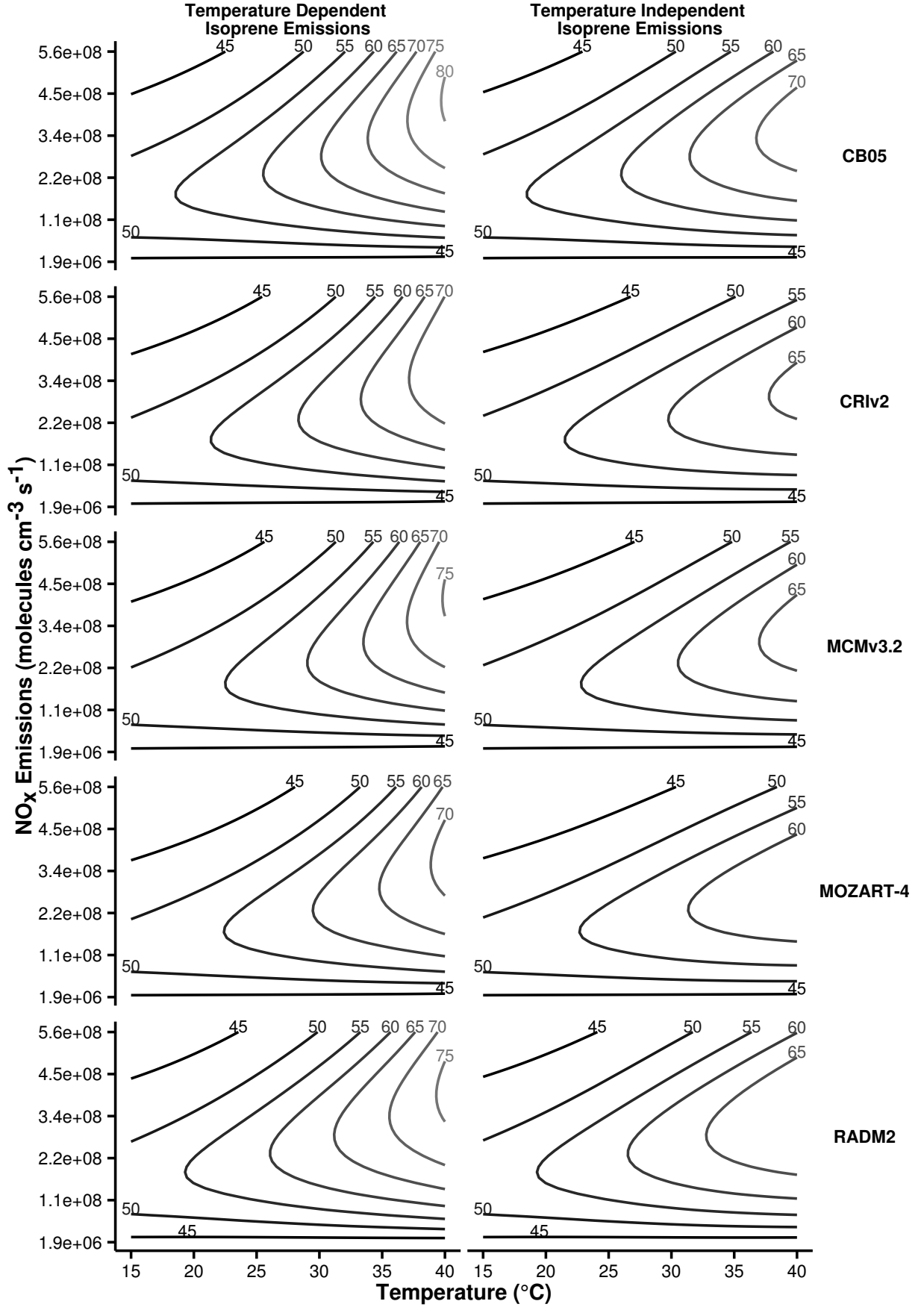
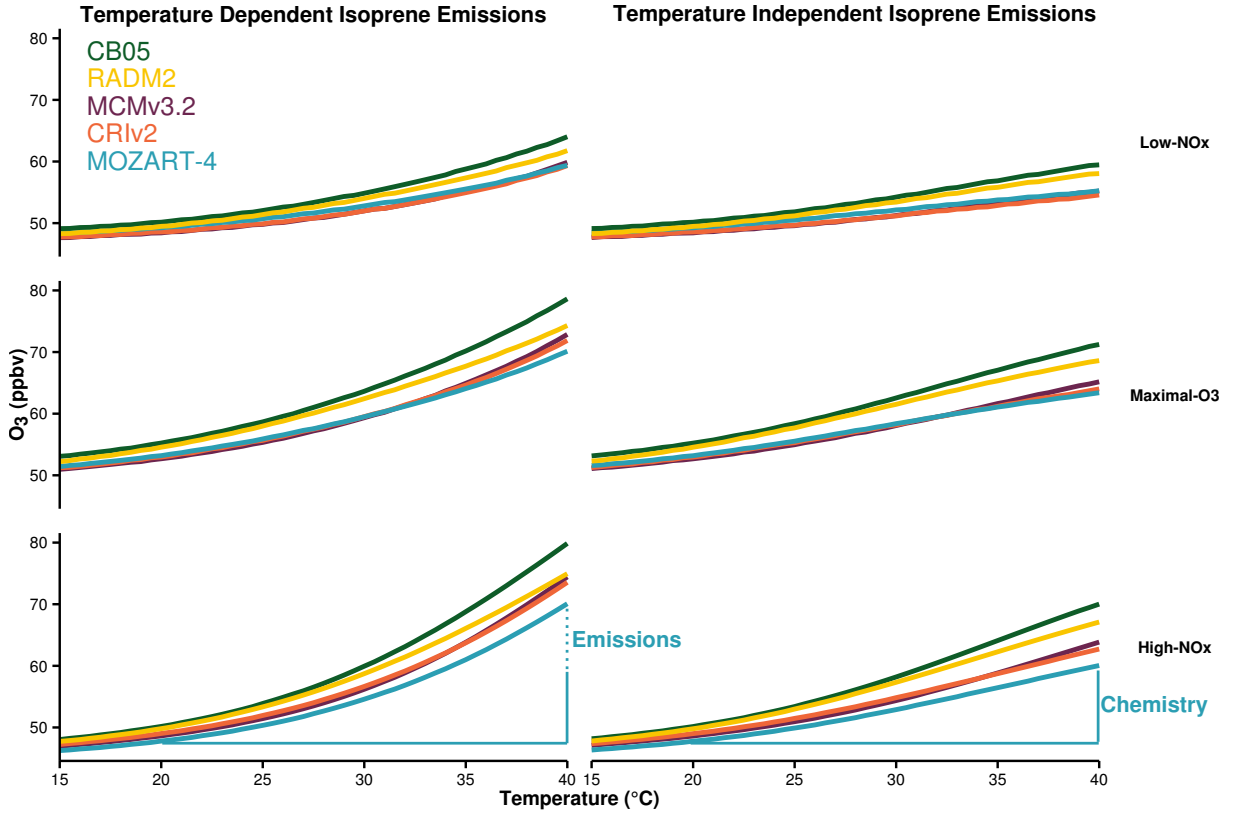




Figure 3: Ozone mixing ratios (ppbv) at each temperature are allocated to different  $\text{NO}_x$ -regimes of Fig. 2. The differences in ozone mixing ratios due to chemistry (solid line) and emissions (dotted line) are represented graphically for MOZART-4 with High- $\text{NO}_x$  conditions and summarised in Table 2, the approach was used to calculate the differences with each chemical mechanism.



Maximal- $\text{O}_3$  regime. Pusede et al. (2014) showed that temperature can be used as a proxy for VOC, thus we assigned the ozone mixing ratios from each box model simulation to a  $\text{NO}_x$  regime based on the ratio of  $\text{HNO}_3$  to  $\text{H}_2\text{O}_2$ . This ratio was used by Sillman (1995) to designate ozone to  $\text{NO}_x$  regimes based on  $\text{NO}_x$  and VOC levels.

Fig. 3 illustrates the mean ozone mixing ratio at each temperature in the  $\text{NO}_x$  regimes for each chemical mechanism and each source of isoprene emissions. The absolute increase in ozone at 40  $^{\circ}\text{C}$  from 20  $^{\circ}\text{C}$  due to faster chemistry is the difference between ozone mixing ratios at 40  $^{\circ}\text{C}$  and 20  $^{\circ}\text{C}$  when using a temperature-independent source of isoprene emissions. When using a temperature-dependent source of isoprene emissions, the difference in ozone mixing ratios at 40  $^{\circ}\text{C}$  from 20  $^{\circ}\text{C}$  minus the increase due to faster chemistry, gives the absolute increase in ozone due to increased isoprene emissions. These differences are represented graphically in Fig. 3 and summarised in Table 2.

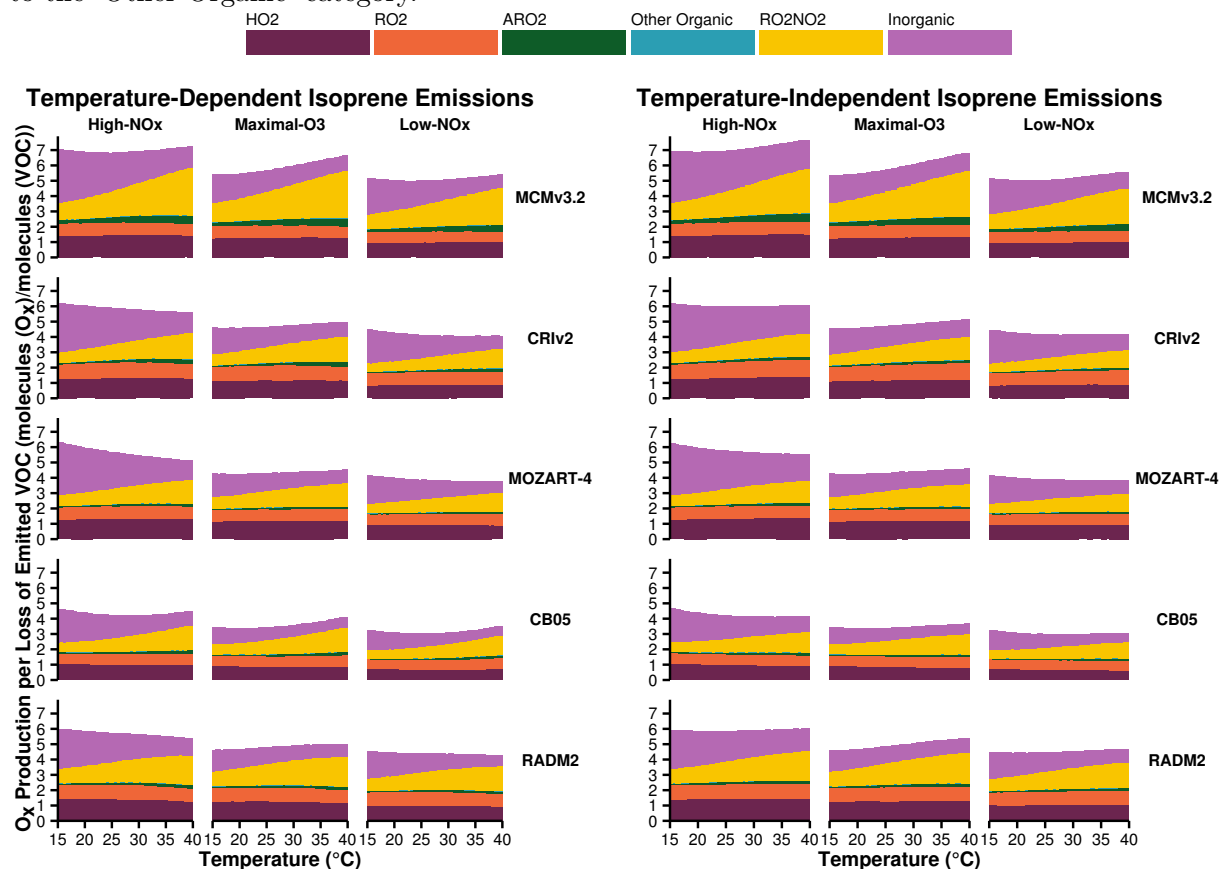
Table 2 shows that the absolute increase in ozone with temperature due to faster chemistry is larger than the absolute increase in ozone due to increased isoprene emissions for each chemical mechanism and each  $\text{NO}_x$  regime. The absolute increase in ozone is largest with High- $\text{NO}_x$

conditions and lowest with Low-NO<sub>x</sub> conditions (Fig. 3 and Table 2). The increase in ozone mixing ratio at 40 °C from 20 °C due to faster chemistry with High-NO<sub>x</sub> conditions is almost double that with Low-NO<sub>x</sub> conditions. We determine the chemical processes responsible for the increases in ozone mixing ratios with temperature by analysing O<sub>x</sub> production budgets in Sect. 3.2.

In the Low-NO<sub>x</sub> regime, the increase of ozone with temperature using the reduced chemical mechanisms (CRIV2, MOZART-4, CB05 and RADM2) is similar to that from the MCMv3.2, larger differences occur in the Maximal-O<sub>3</sub> and High-NO<sub>x</sub> regimes. These differences between the chemical mechanisms shall be explored in Sect. 3.2. All reduced chemical mechanisms except RADM2 have similar increases in ozone due to increased isoprene emissions to MCMv3.2 (Table 2). RADM2 produces 3 ppbv less ozone than the MCMv3.2 due to increased isoprene emissions in each NO<sub>x</sub> regime, indicating that this difference is due the representation of isoprene degradation chemistry in RADM2.

The Tagged Ozone Production Potential (TOPP) defined in Butler et al. (2011) is a measure of the number of molecules of ozone produced per molecule of VOC emitted. Coates and Butler (2015) compared ozone production in different chemical mechanisms to the MCMv3.2 using TOPPs and showed that less ozone is produced per molecule of isoprene emitted using RADM2 than with MCMv3.2. The degradation of isoprene has been extensively studied and it is well-known that methyl vinyl ketone (MVK) and methacrolein are signatures of isoprene degradation (Atkinson, 2000). All chemical mechanisms in our study except RADM2 explicitly represent MVK and methacrolein (or in the case of CB05, a lumped species representing both these secondary degradation products). RADM2 does not represent methacrolein and the mechanism species representing ketones (KET) is a mixture of acetone and methyl ethyl ketone (MEK) (Stockwell et al., 1990). Thus the secondary degradation of isoprene in RADM2 is unable to represent the ozone production from the further degradation of the signature secondary degradation products of isoprene, MVK and methacrolein. Updated versions of RADM2, RACM (Stockwell et al., 1997) and RACM2 (Goliff et al., 2013), sequentially included methacrolein and MVK and with these updates the TOPP value of isoprene approached that of the MCMv3.2 (Coates and Butler, 2015).

Figure 4: Day-time  $O_x$  production budgets normalised by the total oxidation rate of emitted VOC in the  $NO_x$ -regimes of Fig. 3. The budgets are allocated to categories of inorganic reactions, peroxy nitrate ( $RO_2NO_2$ ) decomposition, reactions of  $NO$  with  $HO_2$ , alkyl peroxy radicals ( $RO_2$ ) and acyl peroxy radicals ( $ARO_2$ ). All other reactions contributing to  $O_x$  budgets are allocated to the ‘Other Organic’ category.



### 3.2 Ozone Production Budgets

The total day-time production budgets of  $O_x$  ( $\equiv O_3 + NO_2 + O$ ) normalised by the total rate of oxidation of the emitted VOC are displayed in Fig. 4. The  $O_x$  production budgets are assigned to each  $NO_x$  regime for each chemical mechanism and source of isoprene emissions. The budgets are allocated to the major sources, where ‘ $HO_2$ ’, ‘ $RO_2$ ’, ‘ $ARO_2$ ’ represent the reactions of  $NO$  with  $HO_2$ , alkyl peroxy radicals and acyl peroxy radicals respectively. ‘ $RO_2NO_2$ ’ represents the thermal decomposition of peroxy nitrates, ‘Inorganic’ represents all inorganic contributions to  $O_x$  production (primarily the de-excitation of  $O^1D$  to  $O$ ) and any other remaining organic reactions producing  $O_x$  are included in the ‘Other Organic’ category.

In Fig. 4, a similar number of molecules of  $O_x$  per molecule of emitted VOC oxidised are produced in High- $NO_x$  conditions when using either temperature-dependent or temperature-independent isoprene emissions for each chemical mechanism, the same occurs for the Maximal- $O_3$  and Low- $NO_x$  regimes. Thus the increases in ozone production due to increased

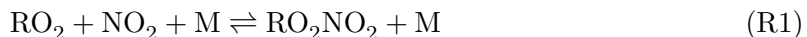
emissions of isoprene with temperature are balanced by the faster oxidation rates at higher temperatures. The largest amount of  $O_x$  is produced in the High- $NO_x$  regime and the lowest amount of  $O_x$  is produced in the Low- $NO_x$  regime, mirroring the  $O_3$  mixing ratios in the different  $NO_x$  regimes in Fig. 3. For example, MCMv3.2 produces seven molecules of  $O_x$  per molecule of emitted VOC oxidised in High- $NO_x$  conditions decreasing to about six and five molecules of  $O_x$  per molecule of emitted VOC oxidised in the Maximal- $O_3$  and Low- $NO_x$  regimes.

Thermal decomposition of  $RO_2NO_2$  contributes the most to the normalised  $O_x$  production at higher temperatures in Fig. 4, this contribution shows a strong dependency on temperature and is analysed further in Sect. 3.2.1. The contributions of the reaction of NO with peroxy radicals ( $HO_2$ ,  $RO_2$  and  $ARO_2$  in Fig. 4) to the normalised production of  $O_x$  do not increase strongly with temperature indicating that the faster oxidation of emitted VOC at higher temperatures produces more peroxy radicals which when reacting NO fuels  $O_x$  production.

The reduced chemical mechanisms produce up to two molecules of  $O_x$  per molecule of emitted VOC oxidised less than the MCMv3.2 in each  $NO_x$  regime despite the reduced chemical mechanisms producing similar absolute amounts of ozone to the MCMv3.2 (Fig. 2 and Fig. 3). At high temperatures, up to 86 % of the total difference in the normalised  $O_x$  production using the reduced chemical mechanisms from the MCMv3.2 is due to differences in the contribution from peroxy nitrate ( $RO_2NO_2$ ) decomposition. These differences shall be explored in more detail in Sect. 3.2.1.

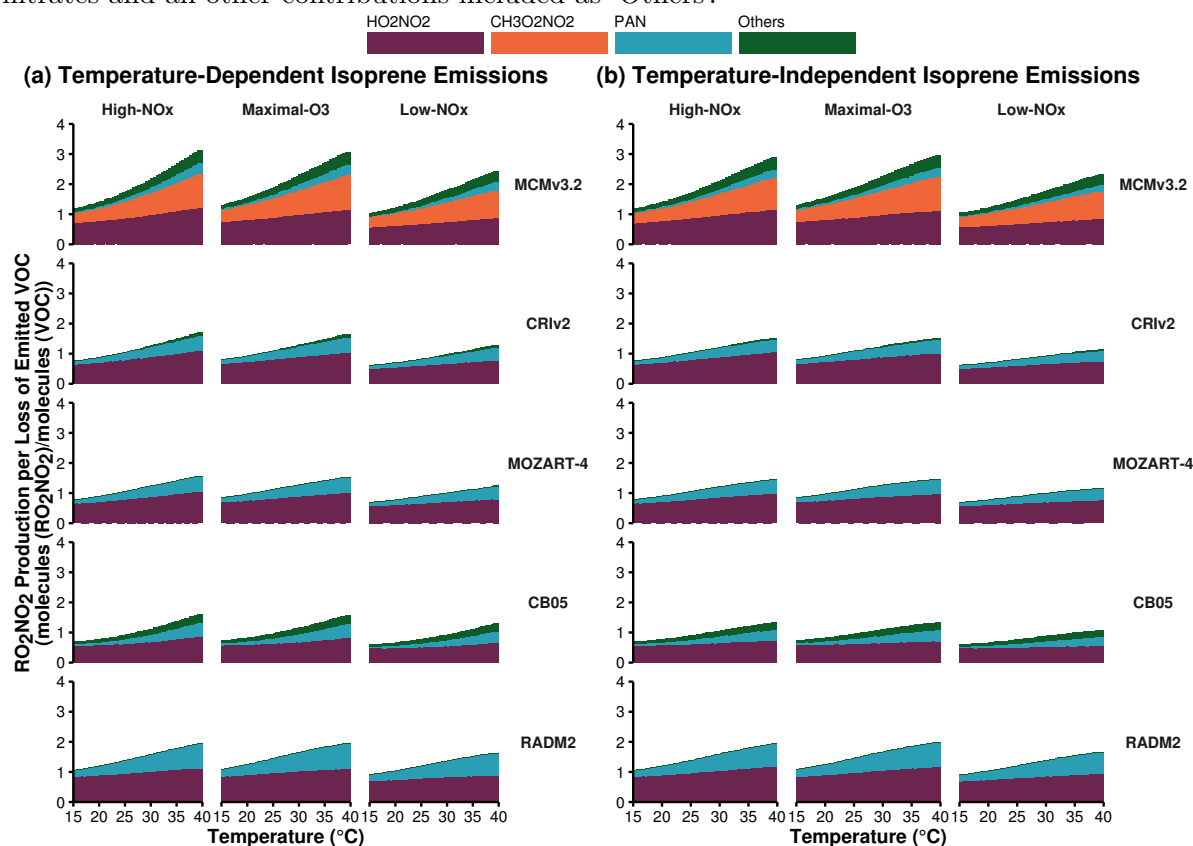
### 3.2.1 Peroxy Nitrates

Peroxy nitrates are formed from the reactions of peroxy radicals ( $RO_2$ ) with  $NO_2$  (R1) and are an important reservoir species for both peroxy radicals and  $NO_x$ .



The chemical bond of  $RO_2NO_2$  is relatively weak and thermal decomposition is the most important chemical process with the rate of thermal decomposition increasing strongly with temperature. At low temperatures,  $RO_2NO_2$  can accumulate and be transported downwind of the emissions of the sources of its precursors (VOC and  $NO_x$ ) and after thermal decomposition the release of  $NO_2$  and peroxy radicals can promote production of  $O_3$  in regions devoid of large  $NO_x$  sources (Moxim et al., 1996).

Figure 5: Day-time  $\text{RO}_2\text{NO}_2$  production budgets normalised by the total oxidation rate of emitted VOC in the  $\text{NO}_x$ -regimes of Fig. 3. The total budgets are allocated to the most important peroxy nitrates and all other contributions included as ‘Others’.



Peroxy nitrates are formed from both alkyl and acyl peroxy radicals produced during the secondary degradation of emitted VOC. The most important alkyl peroxy nitrates are pernitric acid ( $\text{HO}_2\text{NO}_2$ ) and methylperoxy nitrate ( $\text{CH}_3\text{O}_2\text{NO}_2$ ), while peroxy acetyl nitrate (PAN,  $\text{CH}_3\text{C}(\text{O})\text{O}_2\text{NO}_2$ ) and peroxy propionyl nitrate (PPN,  $\text{C}_2\text{H}_5\text{C}(\text{O})\text{O}_2\text{NO}_2$ ) are important acyl peroxy nitrates. The alkyl peroxy nitrates have a weaker  $\text{RO}_2\text{—NO}_2$  bond than acyl peroxy nitrates hence alkyl peroxy nitrates have a shorter lifetime than acyl peroxy nitrates. At 298 K, the lifetime of  $\text{CH}_3\text{O}_2\text{NO}_2$  is 0.5 seconds while PAN has a lifetime of 51 minutes (Orlando and Tyndall, 2012).

Each chemical mechanism used in our study represents  $\text{HO}_2\text{NO}_2$  and PAN, although in many reduced chemical mechanisms the PAN mechanism species represents  $\text{CH}_3\text{C}(\text{O})\text{O}_2\text{NO}_2$  and other acyl peroxy nitrates. This representation of PAN in reduced chemical mechanisms can overestimate PAN levels compared to more detailed chemical mechanisms (Luecken et al., 1999). The near-explicit MCMv3.2 represents a range of peroxy nitrates including  $\text{CH}_3\text{O}_2\text{NO}_2$  and about 280 acyl peroxy nitrates.

Figure 5 displays the normalised production budgets of  $\text{RO}_2\text{NO}_2$  by the total oxidation

Table 3: Slopes ( $m_{O_3-T}$  in ppbv per  $^{\circ}C$ ) of the linear fit to the ozone-temperature correlations in Fig. 6

(a) Slope of linear fit of the ERA-Interim observational data and WRF-Chem model output using MOZART-4 and RADM2 chemistry over central and eastern Germany and western and central Poland.

	Germany	Poland
ERA-Interim	2.15	1.94
WRF-Chem with MOZART-4	2.05	2.00
WRF-Chem with RADM2	1.78	1.77

(b) Slope of linear fit of box model experiments for each chemical mechanism, source of isoprene emissions allocated to the three  $NO_x$ -regimes.

Mechanism	Isoprene Emissions	Low- $NO_x$	Maximal- $O_3$	High- $NO_x$
MCMv3.2	Temperature Dependent	0.42	0.74	0.93
	Temperature Independent	0.28	0.51	0.59
CRIv2	Temperature Dependent	0.40	0.71	0.90
	Temperature Independent	0.25	0.47	0.55
MOZART-4	Temperature Dependent	0.38	0.65	0.81
	Temperature Independent	0.25	0.44	0.49
CB05	Temperature Dependent	0.52	0.89	1.12
	Temperature Independent	0.39	0.67	0.79
RADM2	Temperature Dependent	0.48	0.79	0.97
	Temperature Independent	0.37	0.61	0.70

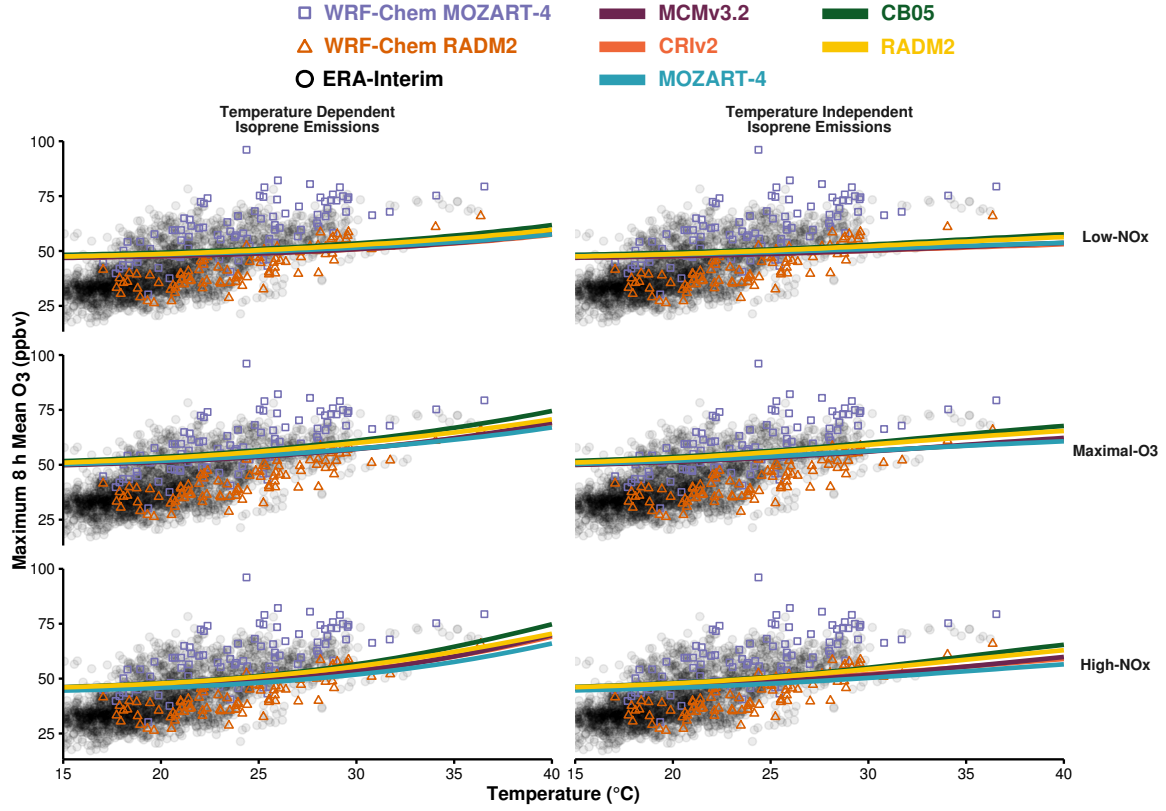
rate of the emitted VOC for each chemical mechanism in each  $NO_x$  regime with a temperature-independent and temperature-dependent source of isoprene emissions. The contribution of  $CH_3O_2NO_2$  to normalised  $RO_2NO_2$  production in MCMv3.2 is missing from the budgets of each reduced chemical mechanism as  $CH_3O_2NO_2$  is not represented in any of the reduced chemical mechanisms. In fact when removing the contribution of  $CH_3O_2NO_2$  to normalised  $RO_2NO_2$  production in MCMv3.2, the normalised  $RO_2NO_2$  production of the reduced chemical mechanisms is similar to that in the MCMv3.2 for each  $NO_x$  regime and regardless of isoprene source. Including  $CH_3O_2NO_2$  chemistry in reduced chemical mechanisms would improve the representation of the total  $RO_2NO_2$  production having the added benefit of improving the representation of  $O_x$  production budgets in Fig. 4.

### 3.3 Comparison to Observations and 3D Model Simulations

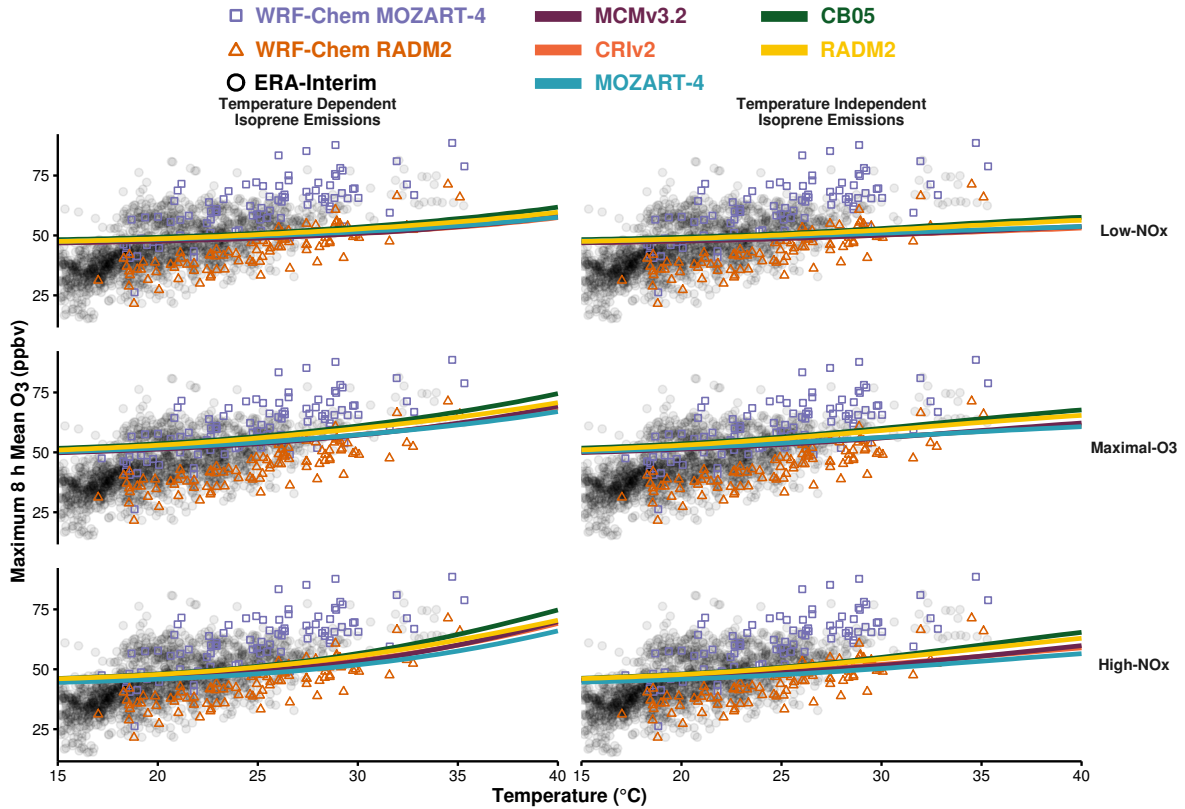
This section compares the results from our idealised box model simulations to real-world observations and model output from a 3D model. Otero et al. (2016) showed that over the summer (JJA) months, temperature is the main meteorological driver of ozone production over

Figure 6: The maximum 8 h mean ozone from the box model simulations allocated to the different  $\text{NO}_x$  regimes for each chemical mechanisms (solid lines). The box model ozone-temperature correlation is compared to the summer 2007 ERA-Interim data (black circles) and WRF-Chem output using MOZART-4 (purple boxes) and RADM2 (orange triangles).

(a) Ozone-Temperature correlation over central and eastern Germany



(b) Ozone-Temperature correlation over central and western Poland



many regions of central Europe using the observational data set of the ERA-Interim re-analysis of Schnell et al. (2015). This data set includes the daily maximum temperature and daily maximum 8 h mean of ozone for the years 1998–2012 over Europe. Model output from the 3D WRF-Chem regional model set-up over the European domain for simulations of the year 2007 using MOZART-4 and RADM2 chemistry from Mar (2015) was used to further compare the box model simulations to a model including more meteorological processes than the box model.

Figure 6 compares the observational (ERA-Interim) and WRF-Chem data from summer 2007 to the maximum 8 h mean ozone from the box model simulations for each chemical mechanism,  $\text{NO}_x$  regime and source of isoprene emissions. In Fig. 6, we limited the observational data to days where the observed daily maximum temperature corresponded to the temperature range in our study (15–40 °C). We selected two regions from the observations and WRF-Chem output, central and eastern Germany (Fig. 6a) and central and western Poland (Fig. 6b), where the summertime ozone values correlated with temperature (Otero et al., 2016). Table 3 summarises the slopes ( $m_{\text{O}_3\text{-T}}$ ) of the linear fits of all the ozone-temperature correlations displayed in Fig. 6 in ppbv of ozone per °C determining the rate of change of ozone with temperature.

The spread of the ERA-Interim ozone-temperature values over both Germany and Poland are generally captured by the combined WRF-Chem simulations with both MOZART-4 and RADM2 chemistry. However, the ozone-temperature data from WRF-Chem using MOZART-4 chemistry reproduces the higher ozone values with temperature from ERA-Interim but not the lower values. On the other hand, WRF-Chem with RADM2 only reproduces the lower ozone values of the ERA-Interim data. The differences between the ozone produced using WRF-Chem with MOZART-4 and RADM2 shall be addressed in Mar (2015). The rate of change of ozone with temperature from the WRF-Chem simulations using both MOZART-4 and RADM2 is similar to the rate of change of ozone with temperature from the ERA-Interim data (Table 3a).

The differences in ozone production between the different chemical mechanisms with the box model are insignificant compared to the spread of the ERA-Interim and WRF-Chem data. When using a temperature-dependent source of isoprene emissions in the box model, the rate of change of ozone with temperature in the box model approaches that of the observed data. The box model simulations using a temperature-independent source of isoprene emissions do not reproduce the range of observed ozone-temperature values (Table 3).

A temperature-dependent source of isoprene with high- $\text{NO}_x$  conditions produces the most similar ozone-temperature slope to the observational data but this is still lower than the observed



ozone-temperature slope by a factor of two. In particular, the box model simulations over-predict the ozone values at lower temperatures and under-predict the ozone values at higher temperatures compared to the ERA-Interim data. Similarly, the rate of change of ozone with temperature in the box model is less-sensitive than WRF-Chem using MOZART-4 or RADM2 chemistry.

The main reason for the box model simulations being less sensitive to temperature than the observations and WRF-Chem simulations is related to the set-up of the box model. Observations and the WRF-Chem simulations consider both the direct and indirect effects of temperature on ozone, while our box model only considered two direct effects of temperature on ozone. Furthermore, observational studies represent at the total derivative of ozone with temperature while models consider the partial derivatives of the temperature-dependent processes influencing ozone (Rasmussen et al., 2013).

$$\frac{d[\text{O}_3]}{dT} = \frac{\partial[\text{O}_3]}{\partial[\text{BVOC}]} \frac{\partial[\text{BVOC}]}{\partial T} + \frac{\partial[\text{O}_3]}{\partial \text{Chemistry}} \frac{\partial \text{Chemistry}}{\partial T} + \frac{\partial[\text{O}_3]}{\partial \text{Stagnation}} \frac{\partial \text{Stagnation}}{\partial T} + \dots$$

In our simulations, we focused on instantaneous production of ozone from a freshly-emitted source of VOC not considering stagnant atmospheric conditions. In these atmospheric conditions, where high temperatures are present for multi-day periods, the ozone from the previous day is not transported away from the region leading to increased ozone levels when including the production of fresh ozone from new emissions. Otero et al. (2016) showed that the previous day’s ozone was also an important driver for observed ozone production over Europe. 3D models such as WRF-Chem that can simulate more realistic atmospheric conditions would play a valuable role for future work evaluating the ozone-temperature relationship at different  $\text{NO}_x$  conditions at a regional scale.

## 4 Conclusions

In this study, we determined the effects of temperature on ozone production using a box model over a range of temperatures and  $\text{NO}_x$  conditions with a temperature-independent and temperature-dependent source of isoprene emissions. These simulations were repeated using reduced chemical mechanism schemes (CRIV2, MOZART-4, CB05 and RADM2) typically used in 3D models and compared to the near-explicit MCMv3.2 chemical mechanism.

Each chemical mechanism produced a non-linear relationship of ozone with temperature and  $\text{NO}_x$  with the most ozone produced at high temperatures and high emissions of  $\text{NO}_x$ . Conversely,

lower NO<sub>x</sub> levels led to a minimal increase of ozone with at all temperatures. Thus air quality in a future with higher temperatures predicted with climate change would benefit from dramatical reductions in NO<sub>x</sub> emissions.

Faster chemistry at higher temperatures was responsible for a greater absolute increase in ozone than increased isoprene emissions. Faster thermal decomposition of peroxy nitrates at higher temperatures contributed the most to ozone production with each chemical mechanism and all NO<sub>x</sub> conditions. The contribution of peroxy nitrates using reduced chemical mechanisms (CRIV2, MOZART-4, CB05, RADM2) was less than the reference MCMv3.2 chemical mechanisms. The differences were mainly due to the inclusion of methylperoxy nitrate (CH<sub>3</sub>O<sub>2</sub>NO<sub>2</sub>) chemistry in MCMv3.2 that is not included in any of the reduced chemical mechanisms used in this study. Including methylperoxy nitrate chemistry in reduced chemical mechanisms would minimise the differences in the production of ozone from reduced chemical mechanisms to the MCMv3.2 at higher temperatures.

The rate of change of ozone with temperature using observational data (ERA-Interim) over Europe was twice as high as when using the box model. This was due to the box model not representing stagnant atmospheric conditions that are inherently included in observational data and models including meteorology, such as WRF-Chem. Future work looking at the influence of temperature on ozone should include stagnant conditions to represent more realistic atmospheric conditions. Any modelling work addressing this should also consider a range of NO<sub>x</sub> conditions as this strongly influenced the amount of ozone produced in our study.

## References

- Roger Atkinson. Atmospheric chemistry of VOCs and NO<sub>x</sub>. *Atmospheric Environment*, 34(12-14): 2063–2101, 2000.
- A. Baklanov, K. Schlünzen, P. Suppan, J. Baldasano, D. Brunner, S. Aksoyoglu, G. Carmichael, J. Douros, J. Flemming, R. Forkel, S. Galmarini, M. Gauss, G. Grell, M. Hirtl, S. Joffre, O. Jorba, E. Kaas, M. Kaasik, G. Kallos, X. Kong, U. Korsholm, A. Kurganskiy, J. Kushta, U. Lohmann, A. Mahura, A. Manders-Groot, A. Maurizi, N. Moussiopoulos, S. T. Rao, N. Savage, C. Seigneur, R. S. Sokhi, E. Solazzo, S. Solomos, B. Sørensen, G. Tsegas, E. Vignati, B. Vogel, and Y. Zhang. Online coupled regional meteorology chemistry models in Europe: current status and prospects. *Atmospheric Chemistry and Physics*, 14(1):317–398, 2014.

371 T.M. Butler, M.G. Lawrence, D. Taraborrelli, and J. Lelieveld. Multi-day ozone production  
 372 potential of volatile organic compounds calculated with a tagging approach. *Atmospheric*  
 373 *Environment*, 45(24):4082 – 4090, 2011.

374 William P. L. Carter. Development of a Database for Chemical Mechanism Assignments for  
 375 Volatile Organic Emissions. *Journal of the Air & Waste Management Association*, 0, 2015.

376 William P. L. Carter, Arthur M. Winer, Karen R. Darnall, and James N. Pitts Jr. Smog chamber  
 377 studies of temperature effects in photochemical smog. *Environmental Science & Technology*, 13  
 378 (9):1094–1100, 1979.

379 J. Coates and T. M. Butler. A comparison of chemical mechanisms using tagged ozone production  
 380 potential (TOPP) analysis. *Atmospheric Chemistry and Physics*, 15(15):8795–8808, 2015.

381 John P. Dawson, Peter J. Adams, and Spyros N. Pandis. Sensitivity of ozone to summertime  
 382 climate in the eastern USA: A modeling case study . *Atmospheric Environment*, 41(7):1494 –  
 383 1511, 2007.

384 L. K. Emmons, S. Walters, P. G. Hess, J.-F. Lamarque, G. G. Pfister, D. Fillmore, C. Granier,  
 385 A. Guenther, D. Kinnison, T. Laepple, J. Orlando, X. Tie, G. Tyndall, C. Wiedinmyer, S. L.  
 386 Baughcum, and S. Kloster. Description and evaluation of the Model for Ozone and Related  
 387 chemical Tracers, version 4 (MOZART-4). *Geoscientific Model Development*, 3(1):43–67, 2010.

388 Wendy S. Goliff, William R. Stockwell, and Charlene V. Lawson. The regional atmospheric  
 389 chemistry mechanism, version 2. *Atmospheric Environment*, 68:174 – 185, 2013.

390 A. Guenther, T. Karl, P. Harley, C. Wiedinmyer, P. I. Palmer, and C. Geron. Estimates of global  
 391 terrestrial isoprene emissions using MEGAN (Model of Emissions of Gases and Aerosols from  
 392 Nature). *Atmospheric Chemistry and Physics*, 6(11):3181–3210, 2006.

393 A. B. Guenther, X. Jiang, C. L. Heald, T. Sakulyanontvittaya, T. Duhl, L. K. Emmons, and  
 394 X. Wang. The Model of Emissions of Gases and Aerosols from Nature version 2.1 (MEGAN2.1):  
 395 an extended and updated framework for modeling biogenic emissions. *Geoscientific Model*  
 396 *Development*, 5(6):1471–1492, 2012.

397 Shiro Hatakeyama, Hajime Akimoto, and Nobuaki Washida. Effect of temperature on the  
 398 formation of photochemical ozone in a propene-nitrogen oxide (NO<sub>x</sub>)-air-irradiation system.  
 399 *Environmental Science & Technology*, 25(11):1884–1890, 1991.

400 Daniel J. Jacob and Darrell A. Winner. Effect of climate change on air quality. *Atmospheric*  
401 *Environment*, 43(1):51 – 63, 2009. Atmospheric Environment - Fifty Years of Endeavour.

402 M. E. Jenkin, S. M. Saunders, V. Wagner, and M. J. Pilling. Protocol for the development of the  
403 Master Chemical Mechanism, MCM v3 (Part B): tropospheric degradation of aromatic volatile  
404 organic compounds. *Atmospheric Chemistry and Physics*, 3(1):181–193, 2003.

405 M.E. Jenkin, L.A. Watson, S.R. Utembe, and D.E. Shallcross. A Common Representative  
406 Intermediates (CRI) mechanism for VOC degradation. Part 1: Gas phase mechanism development.  
407 *Atmospheric Environment*, 42(31):7185 – 7195, 2008.

408 Michael E. Jenkin, Sandra M. Saunders, and Michael J. Pilling. The tropospheric degradation of  
409 volatile organic compounds: a protocol for mechanism development. *Atmospheric Environment*,  
410 31(1):81 – 104, 1997.

411 J. J. P. Kuenen, A. J. H. Visschedijk, M. Jozwicka, and H. A. C. Denier van der Gon.  
412 TNO-MACC\_II emission inventory; a multi-year (2003–2009) consistent high-resolution european  
413 emission inventory for air quality modelling. *Atmospheric Chemistry and Physics*, 14(20):  
414 10963–10976, 2014.

415 D.J. Luecken, G.S. Tonnesen, J.E. Sickles, and II. Differences in NO<sub>y</sub> speciation predicted by  
416 three photochemical mechanisms. *Atmospheric Environment*, 33(7):1073 – 1084, 1999.

417 Kathleen A. Mar. WRF-Chem Simulations over Europe: Model Evaluation and Chemical  
418 Mechanism Comparison. *In Preparation*, 2015.

419 W. J. Moxim, H. Levy, and P. S. Kasibhatla. Simulated global tropospheric PAN: Its transport  
420 and impact on NO<sub>x</sub>. *Journal of Geophysical Research: Atmospheres*, 101(D7):12621–12638, 1996.

421 John J. Orlando and Geoffrey S. Tyndall. Laboratory studies of organic peroxy radical chemistry:  
422 an overview with emphasis on recent issues of atmospheric significance. *Chem. Soc. Rev.*, 41:  
423 6294–6317, 2012.

424 N. Otero, J. Sillmann, J. L. Schnell, H. W. Rust, and T. Butler. Synoptic and meteorological  
425 drivers of extreme ozone concentrations over europe. *Environmental Research Letters*, 11(2):  
426 024005, 2016.

427 N. Passant. Speciation of UK emissions of non-methane volatile organic compounds. Technical  
428 report, DEFRA, Oxon, UK., 2002.

George Pouliot, Hugo A.C. Denier van der Gon, Jeroen Kuenen, Junhua Zhang, Michael D. Moran,  
 and Paul A. Makar. Analysis of the emission inventories and model-ready emission datasets of  
 Europe and North America for phase 2 of the AQMEII project. *Atmospheric Environment*, 115:  
 345–360, 2015.

S. E. Pusede, D. R. Gentner, P. J. Wooldridge, E. C. Browne, A. W. Rollins, K.-E. Min, A. R.  
 Russell, J. Thomas, L. Zhang, W. H. Brune, S. B. Henry, J. P. DiGangi, F. N. Keutsch, S. A.  
 Harrold, J. A. Thornton, M. R. Beaver, J. M. St. Clair, P. O. Wennberg, J. Sanders, X. Ren,  
 T. C. VandenBoer, M. Z. Markovic, A. Guha, R. Weber, A. H. Goldstein, and R. C. Cohen.  
 On the temperature dependence of organic reactivity, nitrogen oxides, ozone production, and  
 the impact of emission controls in San Joaquin Valley, California. *Atmospheric Chemistry and  
 Physics*, 14(7):3373–3395, 2014.

Sally E. Pusede, Allison L. Steiner, and Ronald C. Cohen. Temperature and Recent Trends in  
 the Chemistry of Continental Surface Ozone. *Chemical Reviews*, 115(10):3898–3918, 2015.

D. J. Rasmussen, Jianlin Hu, Abdullah Mahmud, and Michael J. Kleeman. The ozone–climate  
 penalty: Past, present, and future. *Environmental Science & Technology*, 47(24):14258–14266,  
 2013. PMID: 24187951.

Andrew Rickard, Jenny Young, M. J. Pilling, M. E. Jenkin, Stephen Pascoe, and S. M. Saunders.  
 The Master Chemical Mechanism Version MCM v3.2. <http://mcm.leeds.ac.uk/MCMv3.2/>,  
 2015. [Online; accessed 25-March-2015].

Juli I. Rubin, Andrew J. Kean, Robert A. Harley, Dylan B. Millet, and Allen H. Goldstein.  
 Temperature dependence of volatile organic compound evaporative emissions from motor vehicles.  
*Journal of Geophysical Research: Atmospheres*, 111(D3), 2006. D03305.

S. M. Saunders, M. E. Jenkin, R. G. Derwent, and M. J. Pilling. Protocol for the development of  
 the Master Chemical Mechanism, MCM v3 (Part A): tropospheric degradation of non-aromatic  
 volatile organic compounds. *Atmospheric Chemistry and Physics*, 3(1):161–180, 2003.

J. L. Schnell, M. J. Prather, B. Josse, V. Naik, L. W. Horowitz, P. Cameron-Smith, D. Bergmann,  
 G. Zeng, D. A. Plummer, K. Sudo, T. Nagashima, D. T. Shindell, G. Faluvegi, and S. A. Strode.  
 Use of north american and european air quality networks to evaluate global chemistry–climate  
 modeling of surface ozone. *Atmospheric Chemistry and Physics*, 15(18):10581–10596, 2015.

Sanford Sillman. The use of NO<sub>y</sub>, H<sub>2</sub>O<sub>2</sub>, and HNO<sub>3</sub> as indicators for ozone-NO<sub>x</sub>-hydrocarbon sensitivity in urban locations. *Journal of Geophysical Research: Atmospheres*, 100(D7):14175–14188, 1995.

Sanford Sillman. The relation between ozone, NO<sub>x</sub> and hydrocarbons in urban and polluted rural environments. *Atmospheric Environment*, 33(12):1821 – 1845, 1999.

Sanford Sillman and Perry J. Samson. Impact of temperature on oxidant photochemistry in urban, polluted rural and remote environments. *Journal of Geophysical Research: Atmospheres*, 100(D6):11497–11508, 1995.

D. Simpson, A. Benedictow, H. Berge, R. Bergström, L. D. Emberson, H. Fagerli, C. R. Flechard, G. D. Hayman, M. Gauss, J. E. Jonson, M. E. Jenkin, A. Nyíri, C. Richter, V. S. Semeena, S. Tsyro, J.-P. Tuovinen, Á. Valdebenito, and P. Wind. The EMEP MSC-W chemical transport model – technical description. *Atmospheric Chemistry and Physics*, 12(16):7825–7865, 2012.

William R. Stockwell, Paulette Middleton, Julius S. Chang, and Xiaoyan Tang. The second generation regional acid deposition model chemical mechanism for regional air quality modeling. *Journal of Geophysical Research: Atmospheres*, 95(D10):16343–16367, 1990.

William R. Stockwell, Frank Kirchner, Michael Kuhn, and Stephan Seefeld. A new mechanism for regional atmospheric chemistry modeling. *Journal of Geophysical Research: Atmospheres*, 102(D22):25847–25879, 1997.

E. von Schneidemesser, J. Coates, A. J. H. Visschedijk, H. A. C. Denier van der Gon, and T. M. Butler. Variation of the NMVOC speciation in the solvent sector and the sensitivity of modelled tropospheric ozone. *Submitted for Publication*, 2015a.

Erika von Schneidemesser, Paul S. Monks, James D. Allan, Lori Bruhwiler, Piers Forster, David Fowler, Axel Lauer, William T. Morgan, Pauli Paasonen, Mattia Righi, Katerina Sindelarova, and Mark A. Sutton. Chemistry and the Linkages between Air Quality and Climate Change. *Chemical Reviews*, 2015b. PMID: 25926133.

Patrick Wagner and Wilhelm Kuttler. Biogenic and anthropogenic isoprene in the near-surface urban atmosphere — A case study in Essen, Germany. *Science of The Total Environment*, 475:104 – 115, 2014.

486 Greg Yarwood, Sunja Rao, Mark Yocke, and Gary Z. Whitten. Updates to the Carbon Bond  
487 Chemical Mechanism: CB05. Technical report, U. S Environmental Protection Agency, 2005.